Biophysical Chemistry 185 (2014) 39–46

Contents lists available at ScienceDirect

Biophysical Chemistry

journal homepage: http://www.elsevier.com/locate/biophyschem

Self-assemblies of tricationic porphyrin on inorganic polyphosphate

Victor N. Zozulya [a], Olga A. Ryazanova [a,*], Igor M. Voloshin [a], Mykola M. Ilchenko [b], Igor Ya. Dubey [b], Alexander Yu. Glamazda [a], Victor A. Karachevtsev [a]

[a] Department of Molecular Biophysics, B. Verkin Institute for Low Temperature Physics and Engineering, National Academy of Sciences of Ukraine, 47 Lenin ave, 61103 Kharkov, Ukraine
[b] Department of Synthetic Bioregulators, Institute of Molecular Biology and Genetics, National Academy of Sciences of Ukraine, 150 Zabolotnogo str., 03680 Kyiv, Ukraine

HIGHLIGHTS

- Inorganic polyphosphate induces the self-assembly of tricationic *meso*-porphyrin.
- The aggregates formed are very stable and extended (several hundred nanometers in diameter).
- Porphyrin self-assembly corresponds to the mixture of *J*- and *H*-aggregates.
- Possible structures of porphyrin–polyphosphate complexes were calculated.

GRAPHICAL ABSTRACT

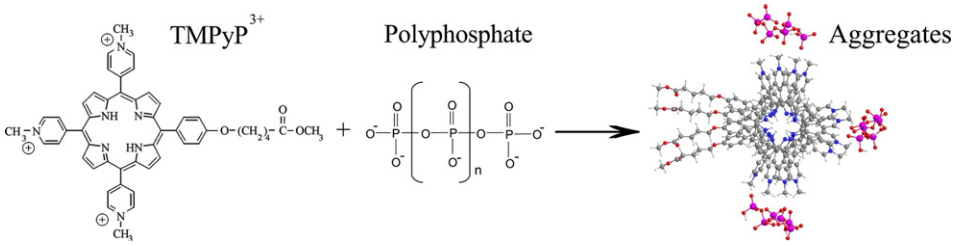

ARTICLE INFO

Article history:
Received 24 October 2013
Received in revised form 18 November 2013
Accepted 18 November 2013
Available online 26 November 2013

Keywords:
Cationic *meso*-porphyrin
Porphyrin aggregation
Polyphosphate
Polarized fluorescence
Light scattering
Absorption

ABSTRACT

Self-assemblies formed by the new synthesized tricationic porphyrin derivative ($TMPyP^{3+}$) on the polyanionic inorganic polyphosphate (PPS) in aqueous solution were studied using different spectroscopic techniques and DFT calculation method. From the fluorescence quenching of the bound $TMPyP^{3+}$ molecules and their Raman spectra we conclude that porphyrin chromophores form the stable π–π stacking-assemblies onto PPS polyanions. The transformation of the Soret band in absorption spectra at different PPS/$TMPyP^{3+}$concentration ratios evidences that the assemblies are mixtures of *J*- and *H*-aggregates. Molecular modeling performed shows that the flexibility of PPS strand allows a realization of spiral or "face-to-face" one-dimensional structures formed by porphyrin molecules arranged in parallel and antiparallel modes. The peculiarity of PPS structure allows a formation of two porphyrin stacks on opposite sides of polymer strands that result in the appearance of higher-order aggregates. Their size was estimated from the light scattering data. Distinctions between $TMPyP^{3+}$ and TMPyP4 aggregation on PPS template are discussed.

1. Introduction

The self-assembly of meso-substituted porphyrins on different polymer scaffolds attracts essential scientists' attention due to their unique photophysical properties and potential applications in nanomedicine and nanotechnology including design of new photonic materials and devices, fabrication of light-harvesting systems etc. [1,2].

Meso-substituted tris(*N*-methylpyridinium) porphyrin ($TMPyP^{3+}$) is a tricationic analog of well-known symmetric tetracationic porphyrin TMPyP4, which can be easily functionalized, e.g. with a carboxyalkyl group, to allow the covalent attachment of other molecules. In recent years a conjugation of $TMPyP^{3+}$ with various ligands was used to achieve the selective stabilization of G-quadruplex structure of telomeric DNA [3–5], as well as for the development of efficient chemical nucleases [6,7] and photocleavage agents of DNA [8,9]. TMPyP4 is a classic G-quadruplex DNA binder, telomerase inhibitor and thus an efficient anticancer agent [10,11]. We have recently found that telomerase inhibiting activity of $TMPyP^{3+}$ *in vitro* is very close to that of TMPyP4 [12]. While the latter is hardly conjugated to transport polymers or nanoparticles, the attachment of $TMPyP^{3+}$ to polymeric carriers via a suitable cleavable linker can be easily performed. That would result in the development of an efficient antitumor agent with selective delivery

* Corresponding author at: 47 Lenin ave, 61103 Kharkov, Ukraine. Tel.: +380 57 3410958; fax: +380 57 3403370.
E-mail address: ryazanova@ilt.kharkov.ua (O.A. Ryazanova).

0301-4622/$ – see front matter © 2013 Elsevier B.V. All rights reserved.
http://dx.doi.org/10.1016/j.bpc.2013.11.006

to cancer cells. Covalent attachment of low-molecular drugs to natural or synthetic polymeric materials is currently considered a versatile way to improve their therapeutic efficiency and specificity [13]. Upon the porphyrin-carrier linker cleavage inside the target cell, bioactive $TMPyP^{3+}$ would be released being able to bind to the telomeric DNA and to inhibit the telomerase activity. We have studied just this derivative with aliphatic substituent that would form upon the cleavage of tricationic porphyrin conjugates.

Upon binding of the above compound to DNA a self-association of the porphyrin can occur which must be taken into account when analyzing the complex formation. However while the characteristics of di- and tetracationic porphyrins assemblies formed on DNA anionic backbone are well established [14–16], the stacking-aggregation of tricationic porphyrins like $TMPyP^{3+}$ has not yet been studied. It would be important e.g. for the understanding of the mechanism of biological activity of this compound inside the cell, including the interaction with nucleic acids. Moreover, the properties of supramolecular self-assemblies of $TMPyP^{3+}$ are of significant interest in its own right for the physics of porphyrin aggregation.

In the present work we have investigated the interaction of new synthesized $TMPyP^{3+}$ derivative bearing a carboxyalkyl linker with polyanionic matrix of inorganic polyphosphate (PPS) which can simulate the electrostatic interaction of the porphyrin with anionic DNA backbone. The last supposition is based on the fact that PPS chains can assume a conformation where negatively charged PO_2^- groups draw up in rows having the intercharge distance which is close to that in the DNA backbone. We have found that two types of molecular aggregates are formed upon the porphyrin binding to PPS, namely, *J* and *H* one-dimensional stacking-assemblies. Molecular modeling was performed to construct the geometries of the porphyrin stacks. Besides, it was revealed that stacking-aggregates and PPS strands are combined into higher-order aggregates. Spectroscopic and structural characteristics of the aggregates were studied. To reveal the distinction between PPS induced aggregation of $TMPyP^{3+}$ and TMPyP4, we have performed the experimental investigation using the same techniques and under the similar conditions as it was made earlier [17].

2. Experimental

Tris(4-*N*-methylpyridinium)porphyrin carrying the carboxyalkyl chain ($TMPyP^{3+}$, Fig. 1A) was synthesized as previously reported [18]. Sodium polyphosphate (PPS, Fig. 1B) with degree of polymerization approximately 75 was purchased from Sigma Chemical Co. The deionized water from Millipore-Q system was used as a solvent for all sample preparations. The porphyrin concentration was determined spectrophotometrically in water using the extinction coefficient of $\varepsilon_{424} = 200{,}000\ M^{-1}\ cm^{-1}$ at the Soret band maximum [18]. The PPS concentration was estimated from the dissolved substance weight (1% solution corresponds to 98 mM phosphates).

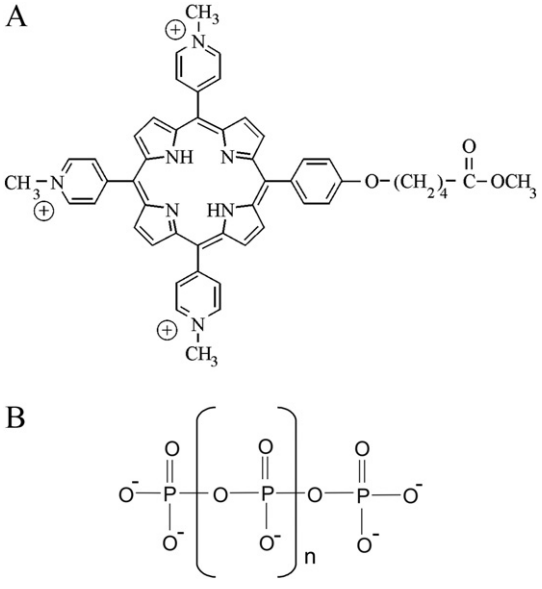

Fig. 1. Molecular structure of tricationic porphyrin derivative $TMPyP^{3+}$ (A) and polyanionic chain of inorganic polyphosphate (B).

The investigations were carried using techniques of polarized fluorescence, absorption, resonance Raman spectroscopy and static light scattering. The spectral equipments and methods of measurements were described in our previous article devoted to investigation of the tetracationic porphyrin TMPyP4 interaction with PPS [17]. The binding of $TMPyP^{3+}$ to PPS was followed by changes in parameters of the porphyrin fluorescence under titration experiments. The fluorescence of the porphyrin was excited at $\lambda_{exc} = 505$ nm and its intensity and polarization were registered at $\lambda_{obs} = 700$ nm (the emission spectral slit was 1 nm). Fluorescence spectra were corrected for spectral sensitivity of the spectrofluorimeter. The aggregation process arisen in the solutions was followed by the intensity of steady-state light scattering (LS) excited and measured at $\lambda_{obs} = 525$ nm corresponding to the wavelength of Q absorption band maximum. Resonance Raman spectra were excited by the emission of 457.9 nm line of an Ar ion laser (power 25 mW) and recorded using conventional 90° registration geometry. The comparative peak positions in the spectra were determined with an accuracy of 0.3 cm^{-1}.

In titration experiments the sample of $[TMPyP^{3+}] = 10$ μM was added with increasing amounts of the concentrated PPS solution containing the same porphyrin concentration, whereupon fluorescence and LS intensities were measured. The time up to 10 min was required to reach the thermodynamic equilibrium in the system which was verified from the approach to the stability in the fluorescence signal. The aim of titration experiments was to obtain dependences of the fluorescence and LS characteristics on the molar phosphate-to-dye ratio, *P*/*D*. The experiments were performed in deaerated deionized water. All measurements were carried out in quartz cuvettes at room temperature from 22 to 24 °C.

Molecular modeling was performed to construct the geometries of the aggregates formed. All calculations were carried out by DFT (Density Functional Theory) approach using M06-2X functional [19] that was proposed for the correct representation of energetics and geometry of π-stacking complexes. Complexes of four $TMPyP^{3+}$ molecules with two or three hexaphosphate chains were investigated. Taking into account the complexity of the studied systems that contain about 500 atoms and 5000 basic functions, we have used 6-31G(d) basic set. Calculations were performed with Gaussian 09 package (revision A.01) provided by the Mississippi Center for Supercomputing Research, USA [20]. Full geometry optimization was performed for each atom of the system in water solution. Threshold value of each of the four main criteria of the procedure of geometry optimization was increased twice. The solvent effects were treated using CPCM (Conductor-like Polarizable Continuum Model) method [21,22].

3. Results and discussion

3.1. Absorption and fluorescent characteristics of the porphyrin aggregate

Visible absorption (Fig. 2) and fluorescence spectra (Fig. 3) of free $TMPyP^{3+}$ and in the complex with inorganic polyphosphate were recorded in aqueous solution. The dye concentration was 10 μM in all samples.

As it can be seen from Fig. 2, the spectrum of the free dye is similar to that of TMPyP4, however 3–3.5 nm red shift was observed. It consists of intense Soret band (B-band) at 425.5 nm (extinction $\varepsilon = 200{,}000\ M^{-1}\ cm^{-1}$) and four less intense Q-bands centered at 522 nm, 561 nm, 583.5 and 642.5 nm. Its fluorescence spectrum consists of wide structureless band centered at *ca.* 715 nm (Fig. 3). The

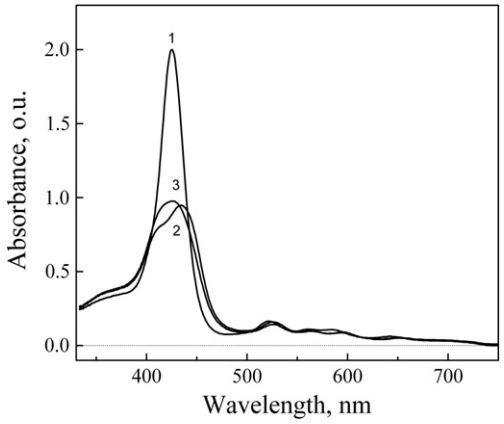

Fig. 2. Normalized absorption spectra of free $TMPyP^{3+}$ porphyrin (1) and bound to polyphosphate one at $P/D = 3.5$ (2) and $P/D = 30$ (3). Measurements were carried out in deionized water, $[TMPyP^{3+}] = 10$ μM.

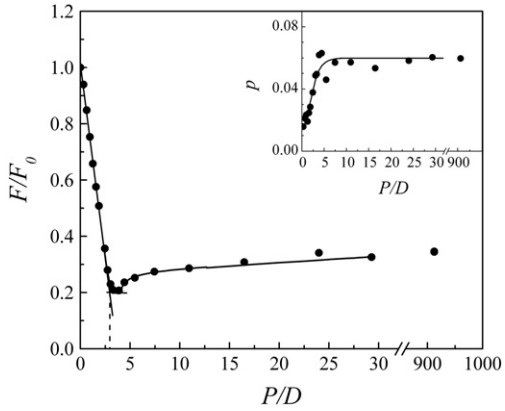

Fig. 4. Dependence of the relative intensity, F/F_0 (F_0 is the fluorescence intensity of the free dye), and polarization degree, p, (inset) of $TMPyP^{3+}$ fluorescence on molar phosphate-to-dye ratio, P/D. The data were obtained in deionized water. The total porphyrin concentration was constant i.e. $[TMPyP^{3+}] = 10$ μM.

fluorescence polarization degree, p, measured at the emission band maximum was found to be around 0.015.

To follow the binding of $TMPyP^{3+}$porphyrin to PPS the fluorescence titration experiments were performed, where changes in the porphyrin relative fluorescence intensity, F/F_0 (here F_0 is fluorescence intensity of the free dye), and polarization degree, p, on P/D were registered at $\lambda_{obs} = 700$ nm (Fig. 4).

As can be seen from Fig. 4, the initial part of the titration curve representing fluorescence intensity changes has the shape typical for strong cooperative binding of cationic dyes to linear polyanions [17,23,24]. Quenching of the dye fluorescence evidences the stacking-association of tricationic porphyrin molecules on PPS polyanionic matrix. At $P/D \approx 3.5$ the fluorescence intensity reaches its minimal ratio $(F/F_0)_{min} = 0.20$. It can be noted that this value remains invariable within experimental error even under the 5-fold reduction in the porphyrin concentration that evidences that the overwhelming majority of porphyrin molecules are involved in the stacking interaction. Thus $(F/F_0)_{min}$ characterizes the emission of properly $TMPyP^{3+}$ stacks. The linear part of the titration curve corresponds to the saturation of PPS binding sites and formation of the extended porphyrin stacking-aggregates. Being extrapolated to the level line of $(F/F_0)_{min}$ it produces the intersection point positioned at $P/D = 3$ (Fig. 4) which determines the stoichiometry of the binding. This obviously means that each $TMPyP^{3+}$ molecule is bound to three negatively charged phosphate groups of PPS.

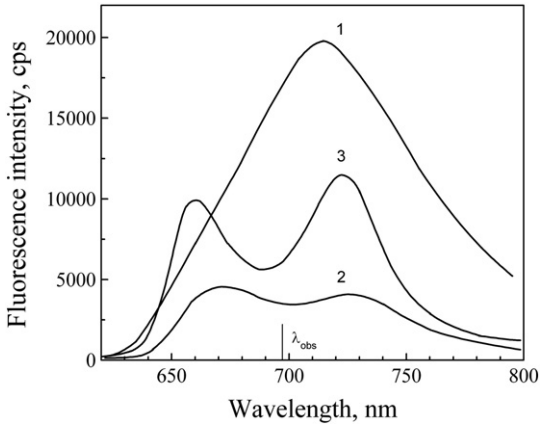

Fig. 3. Fluorescence spectra of free $TMPyP^{3+}$ porphyrin (1) and bound to polyphosphate one at $P/D = 3.5$ (2) and $P/D = 30$ (3). $[TMPyP^{3+}] = 10$ μM; $\lambda_{obs} = 700$ nm is the wavelength where the fluorescence intensity was registered upon the titration experiments.

According to the theory of cooperative binding [25], increase of P/D results in the dissociation of the continuous stacking-aggregates into separate stacks that leads to a gradual decrease in the number of stacked chromophores. In our case the disintegration of the stacks is accompanied by the increase in the fluorescence intensity, which at $P/D \geq 25$ reaches the steady-state level of $F/F_0 \approx 0.34$. It can be supposed that this value is the fluorescent characteristic of very stable $TMPyP^{3+}$ dimers bound to PPS, which do not crumble even at high P/D. At the same time the fluorescence polarization degree increases from $p_0 = 0.015$ (typical for the free dye) up to $p = 0.065 \pm 0.005$ at $P/D \geq 4$ (see inset in Fig. 4), remaining practically constant during further P/D increase. It means that the rotation mobility of bound porphyrin molecules does not depend on the stack size being defined by some another parameters, that will be discussed later.

The absorption and fluorescence spectra of $TMPyP^{3+}$–PPS complexes with $P/D = 3.5$ and 30 are presented in Figs. 2 and 3. We can see that upon the stacking-aggregation of the porphyrin on PPS template the shape of Soret band undergoes some transformation and exhibits a hypochromism of about 53% (Fig. 2). So, at $P/D = 3.5$ where maximal quenching of the porphyrin fluorescence is observed, the profile of the Soret band becomes asymmetric and splitted. New peaks appear on the opposing sides of initial Soret band maximum, at 415 and 443 nm. We suppose that the splitting can be conditioned by the superposition of two bands corresponding to *J*-aggregates (red-shifted one) and *H*-aggregates (blue-shifted one) [26]. The difference in the constituent band intensities is conditioned by the ratio between the concentration of corresponding fractions and the difference in the spectroscopic properties of these aggregates. At $P/D = 30$ the spectrum reflects the absorbance of the porphyrin dimers bound to PPS. We can see (Fig. 2) that the intensity of Soret band is only somewhat higher than that for extended porphyrin stacks ($P/D = 3.5$), however a position of the band maximum is the same as in the case of the free dye ($P/D = 0$).

In the Electronic Supplementary Information (Fig. S1 a,b) we have presented example of the absorption spectra deconvolution performed for free $TMPyP^{3+}$ and its complex with PPS with $P/D = 3.5$. The spectra were fitted by the sums of Gaussian components, corresponding to different porphyrin states, and the relative areas of these components reflect their fractions into the spectrum. As it can be seen in Fig. S1b, relative areas under the Gaussian components in Soret band corresponding to *J*- and *H*-aggregates (bands centered at 443 and 415 nm respectively) are comparable.

Fluorescence spectra of the above mentioned porphyrin–PPS complexes are presented in Fig. 3. It can be seen, that upon the formation of extended porphyrin stacks at $P/D = 3.5$ the fluorescence spectrum splits into two bands centered at *ca.* 670 and 725 nm. At $P/D = 30$ the spectrum splitting becomes more pronounced, and the band peaks are

somewhat shifted toward shorter wavelengths (to *ca.* 661 and 722 nm). Such spectral transformation can be explained by preventing of the intramolecular charge transfer between π-system of porphyrin macrocycle and pyridinium groups caused by the restriction of the rotation of these groups toward coplanar geometry with the porphine ring, as it was described for the $TMPyP^{4+}$ stacking-aggregates [27]. For the bound porphyrin dimers ($P/D \geq 25$) the splitting of the porphyrin fluorescence band can be intensified by the effect of the chromophore nonpolar environment produced by PPS component, as it was observed for TMPyP4 in nonpolar solvents [27]. The ratio between integral intensities of emission calculated for $TMPyP^{3+}$ stacks and free porphyrin (at $P/D = 3.5$ and 0 respectively) as the areas under the corresponding fluorescence bands is amounted to *ca.* 0.125. Approximately the same order of magnitude is expected for its relative fluorescence quantum yield, Q/Q_0, since the emission excitation was performed at 505 nm where absorption of all samples is practically the same. Taking into account that under *H*-aggregation of TMPyP4 porphyrin which chromophore structure is similar to that for $TMPyP^{3+}$ value $Q/Q_0 = 0.23$ was obtained [17], and for its *J*-aggregates the strong fluorescence quenching was observed [28,29] it can be concluded that the obtained magnitude of $Q/Q_0 = 0.125$ is conditioned by the contributions of above two types of the chromophore aggregates into the sample emission.

3.2. Resonance Raman spectra

Resonance Raman (RR) spectra of free $TMPyP^{3+}$ and its complex with PPS at $P/D = 3.5$ (where all bound porphyrin molecules form stacks) were obtained in the range of 300–1900 cm^{-1} (see Fig. 5) where vibrations of pyrrole and pyridyl rings become apparent. The small changes in the pattern of RR spectra upon the porphyrin aggregation were found. The bands corresponding to stretching vibrations of the porphyrin macrocycle at 970 and 1005 cm^{-1} are assigned to $\nu(C_a-C_b)$ and $\nu(C_a-C_m)$, respectively [30] are shifted by 2 cm^{-1} to lower frequencies. These frequency shifts evidence the stacking interaction between the porphyrin core planes. Changes in vibrations attributed to the *N*-methylpyridyl group N^+-CH_3 are also revealed. The frequencies of *N*-methylpyridyl group vibration near 796, 1250 and 1644 cm^{-1} are decreased by 1–2 cm^{-1}. The downward shifts of these RR bands suggest the existence of an electrostatic interaction between N^+-CH_3 groups of porphyrin and PO^- groups of PPS in the aggregates formed. Such small changes in the vibration frequencies (1–2 cm^{-1}) are typical for the noncovalent Coulomb interaction [31]. The essential changes in relative intensities of Raman bands in the spectra are not revealed for the exception of the band at 334 cm^{-1}. This band attributed to bending vibration of the porphyrin macrocycle [30] has been increased approximately by two times that obviously occurred due to a resonance with the excitonic transition that can be occurred in porphyrin molecular aggregates [32].

3.3. Light scattering and aggregation

The drastic increase in the light scattering (LS) intensity has been revealed for the $TMPyP^{3+}$–PPS mixture in the P/D range near the stoichiometric binding ratio (Fig. 6). The phenomenon is conditioned by the aggregation process which was clearly observed visually via a monocular. As can be seen in Fig. 6, in the initial part of the titration curve the LS intensity increases sharply reaching the maximum at the P/D values that correspond to the formation of extended π–π stacking-aggregates. Further P/D increase is accompanied by the slow decrease in LS intensity that evidences that the aggregation process exists even under the high P/D values.

The origin of the aggregation can be explained using the following model. It is supposed that extended columnar $TMPyP^{3+}$ stacks are formed on each PPS strand, and positively charged *N*-methylpyridyl groups of the porphyrin interact electrostatically with negatively charged oxygen atoms of the polymer. By means of the conformation analysis of PPS it was shown that the polyphosphate chain can take both planar (Fig. 7A) and helix conformation [17]. In both these cases negatively charged phosphate groups are arranged along two oppositely situated rows so that the intercharge distance becomes equal to *ca.* 0.42 nm for the planar conformation and 0.36 nm for the helix one. Such arrangement of the negative charges on the polymer promotes formation of two extended porphyrin stacking-aggregates on opposite sides of the PPS chain.

Since the thickness of the porphyrin π-electronic system is equal to 0.34–0.36 nm [33] it can be supposed that the helix PPS conformation induces formation of continuous linear porphyrin *H*-aggregates [17]. In the case of the planar geometry of PPS the planes of the porphyrin macrocycles should be inclined to the stack axis (Fig. 7B) forming "offset card deck" arrangement typical for *J*-aggregates. The above two types of $TMPyP^{3+}$ aggregates manifest themselves in the absorption spectra.

Since each $TMPyP^{3+}$ molecule bears three spatially separated positive charges its stacking-aggregate can join up to three PPS chains. Besides, an ability of each PPS strand to be a template for two porphyrin stacks (Fig. 7B) promotes the integration of adjacent stacks. These mechanisms induce an association of the porphyrin–PPS complexes into higher-order aggregates. The light scattering data evidence that the largest aggregates arise at low P/D values where formation of extended porphyrin stacks occurred. However these aggregates do not disappear even under the stacks decomposition at high P/D, but their size is somewhat decreased. Thus the maximal LS signal observed

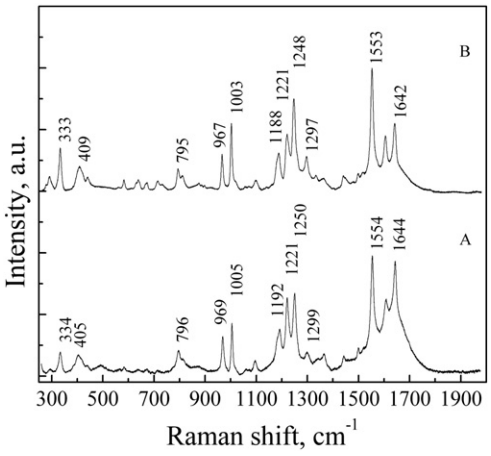

Fig. 5. Fragments of resonance Raman spectra of free $TMPyP^{3+}$ (A) and its complex with PPS recorded at $P/D = 3.5$ (B) where continuous stacking-aggregates are formed. $[TMPyP^{3+}] = 25$ μM.

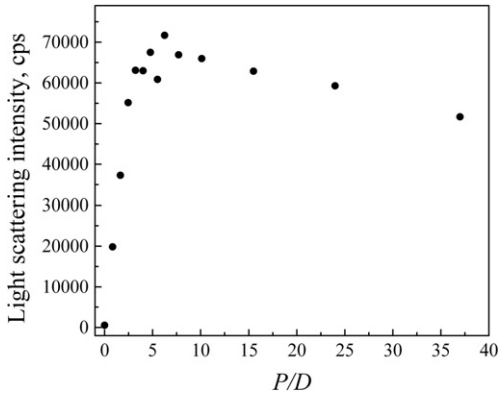

Fig. 6. P/D dependence of the light scattering intensity measured in the $TMPyP^{3+}$–PPS sample at λ = 525 nm. The total porphyrin concentration was constant i.e. $[TMPyP^{3+}] = 10$ μM.

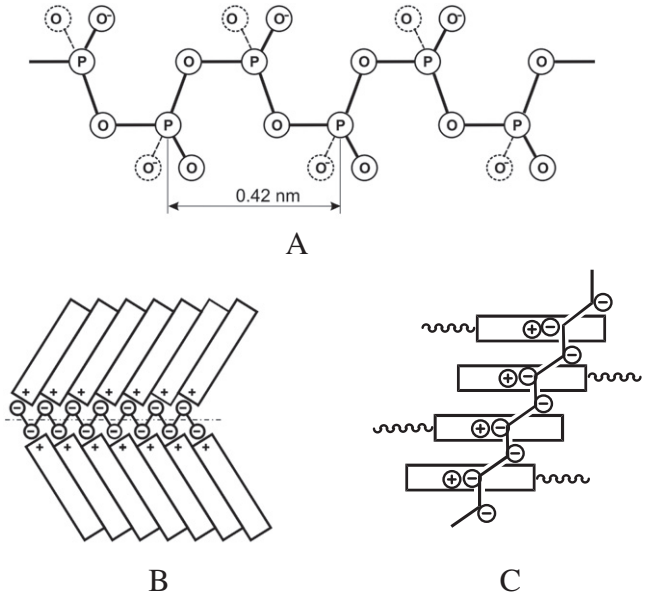

Fig. 7. Scheme of the planar all-trans conformation of PPS chain (A), arrangement of two continuous $TMPyP^{3+}$ stacks on the template of single PPS chain (B), schematic representation of antiparallel $TMPyP^{3+}$ assemblies of the porphyrin on polyphosphate chain (C).

at $P/D \approx 5$ reduces only by ~20% at $P/D = 30$ (Fig. 6). It corresponds to only ~7% decrease in the size of the particles.

We have estimated the size of the aggregates from the solution turbidity data measured for the sample at $P/D = 5$ and applying the method of Doty and Steiner [34], namely, using the equation:

$$-\frac{d\log\tau}{d\log\lambda} = 4 - \frac{d\log Q}{d\log\lambda} = 4 - \beta \quad (1)$$

where τ denotes the turbidity, Q is the particle dissipation factor and λ is the wavelength of the light in vacuum. The dependence of τ on λ was registered by measuring the absorbance in the range of $\lambda = 710$–830 nm, where the porphyrin does not absorb. From the rectilinear plot of $\log\tau$ versus $\log\lambda$ (Fig. 8) a value $d\log\tau/d\log\lambda = -2.9$ was calculated which determines the magnitude of $\beta = 1.1$ in Eq. (1).

Let us consider two cases where the aggregates adopt a conformation (i) of spheres and (ii) of polydisperse coils. Under these assumptions, from Table VII presented in [34] it is followed that the calculated β value corresponds to the ratio $D/\lambda' \approx 0.8$, where D is the coil or sphere diameter and λ' is the mean value of light wavelength in water solution over the measured wavelength range. In our case of $\lambda' \approx 775$ nm, it appears that the diameter of the aggregates, D, is

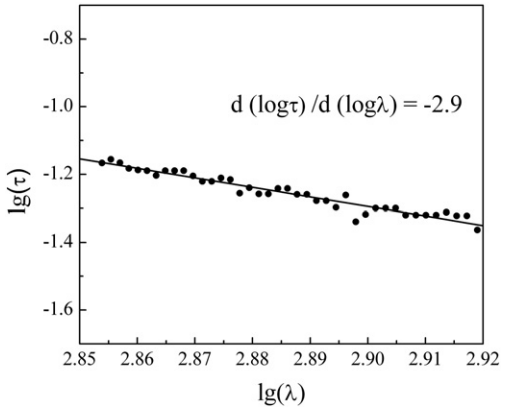

Fig. 8. Wavelength dependence of the solution turbidity for $TMPyP^{3+}$–PPS sample ($P/D = 5$) in water measured in the range of $\lambda = 710$–830 nm.

equal to *ca.* 320 nm in the case of spherical particles, and *ca.* 580 nm for polydisperse coils.

The magnitude of the fluorescence polarization degree, p, gives the information about the rotation mobility of $TMPyP^{3+}$. Upon the aggregation its value increases from $p_0 = 0.015$ for the free porphyrin molecules in water solution up to $p \approx 0.065$ for their complexes with PPS. The independence of p magnitude on P/D over the wide range of the ratios evidences that porphyrin fluorescence polarization degree is defined not only by the stacking association but mainly by the restriction of porphyrin mobility in the higher-order aggregates as a result of its electrostatic binding to PPS strands.

3.4. Models of aggregates

We have used a combination of M06-2X functional and CPCM model to treat the solvent effects. These calculation approaches have been successfully applied before for complex molecular systems. M06-2X functional developed by Zhao and Truhlar quite recently was shown to describe noncovalent interactions better than classic density functionals [19,35]. Among all DFT functionals integrated into Gaussian 09 package, highly parameterized M06-2X is the most appropriate one for the calculation of intermolecular dispersion interactions in large molecular systems. CPCM model is also integrated into Gaussian 09 package and recommended by the developers of Gaussian to be used for the correct estimation of the solvation energy.

Complexes of four $TMPyP^{3+}$ molecules were used for computer modeling as we suppose that this number of the molecules is sufficient for understanding the structure of *J*- and/or *H*-aggregates formed by this porphyrin. Polyphosphate chains were modeled by a fragment containing six PO_2 residues. Positive charges in $TMPyP^{3+}$ are localized at N-methylpyridinium groups, so hexaphosphate chains in the initial structures for optimization were localized at close proximity to these groups. Porphyrin complexes were formed by $TMPyP^{3+}$ molecules assembled in parallel or antiparallel orientation. Polyphosphate chain is sufficiently flexible to adopt in each case a suitable conformation optimal for the interaction. We have calculated the structures of porphyrin quartet stacks with two or three polyphosphate chains. All structures were electroneutral, besides the complex of four porphyrins and three PPS strands (structure 3.1) which has a total charge of (−6).

We have found three main types of complexes formed by $TMPyP^{3+}$ with polyphosphate strands. The structures differ in the arrangement of porphyrin chromophores and the localization of hexamer polyphosphate chains around stacked $TMPyP^{3+}$ arrays. In porphyrin quartets bound to two PPS chains, both parallel and antiparallel $TMPyP^{3+}$ assemblies were found, whereas complex with three polyphosphates contains porphyrin molecules only in parallel orientation. Most favorable structures are presented in Fig. 9 (full data for all calculated structures are presented in the Electronic Supplementary Information, Fig. S2 a–g).

$TMPyP^{3+}$ molecules arranged in antiparallel mode. π−π-Stacking complexes **1.1** and **1.2** are characterized by a small radial turn of porphyrin rings around the vertical axis of the porphyrins stack; there is no horizontal shift of the porphyrins (Fig. S2a, S2b). This spatial arrangement of $TMPyP^{3+}$ molecules allows us to consider these complexes as antiparallel *H*-aggregates. At the same time, structure **1.3** is characterized by a significant horizontal planar shift of porphyrin rings relatively to each other (Fig. S2c). This staircase-type structure can be referred to as the aggregate of *J*-type.

Complexes of the second type (**2.1**–**2.3**) are formed by $TMPyP^{3+}$ molecules arranged in a parallel mode. The spiral turn of porphyrin rings relatively to each other in the quartet is observed. The parallel-type structures allow hydrophobic interaction between alkyl tails which are located in close proximity and form hydrophobic clusters. These complexes somewhat differ in the localization of polyphosphates around the porphyrin stacks, however in all cases PPS binds to the sides of the porphyrins (Fig. S2d–S2f). In all cases electronic π-systems of

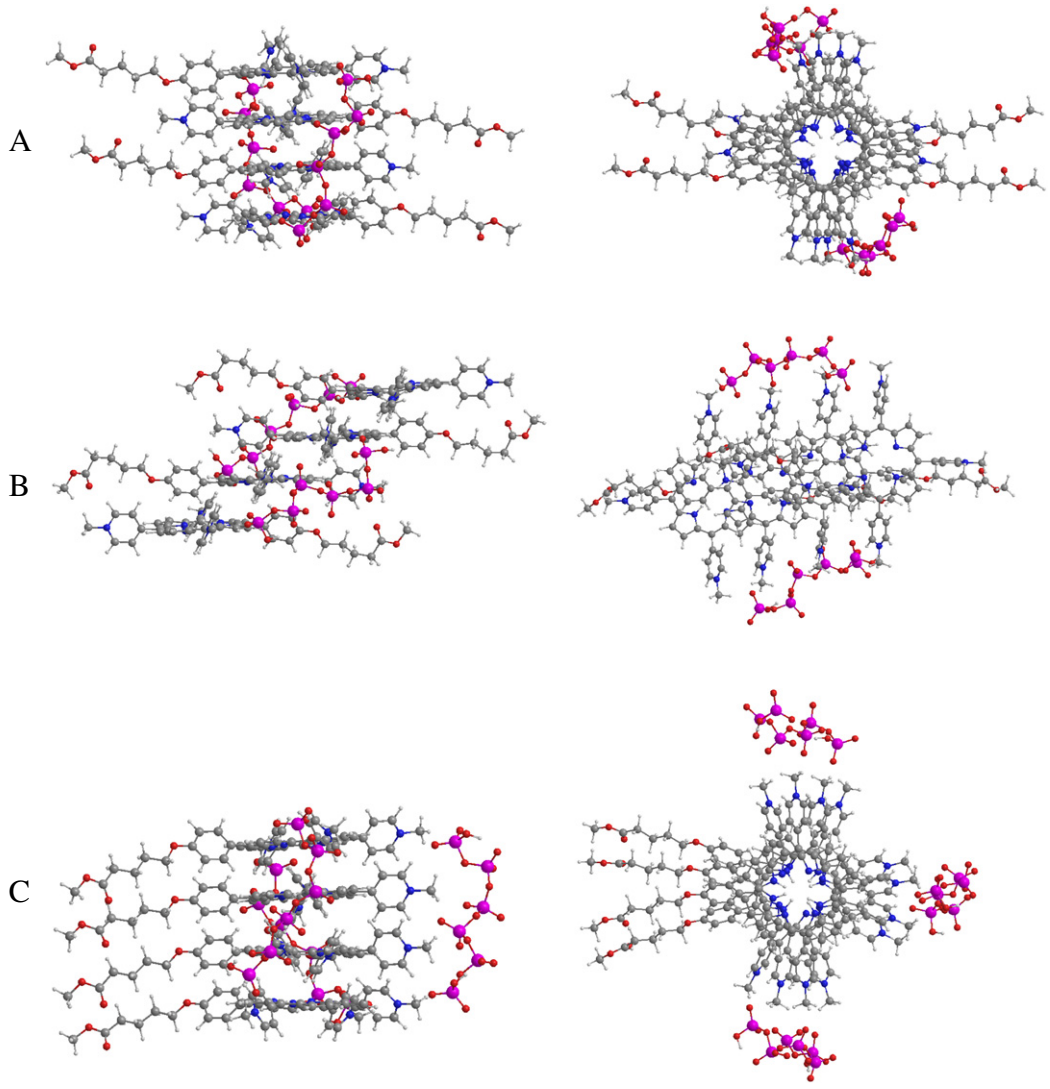

Fig. 9. Side (left) and top (right) views of the most favorable calculated structures of porphyrin-polyphosphate complexes **1.1** (A), **1.3** (B) and **3.1** (C). Carbon atoms are in black, nitrogen — blue, oxygen — red, phosphorus — magenta (see Electronic Supplementary Information).

porphyrin chromophores are well overlapped, thus complexes of this type can be described as parallel *H*-aggregates.

An interesting structure **3.1** was obtained upon theoretical modeling of four-porphyrin stack complex with three polyphosphate chains. In this case, only a parallel-type porphyrin assembly is possible and natural. Stacked porphyrin rings are turned around the vertical axis of the array, and PPS chains form spiral structures around this chiral rod-shaped aggregate (Fig. S2g). All positive charges of porphyrins localized at N-methylpyridinium substituents are neutralized with phosphate anions. The radial turn of porphyrin rings is relatively small and π-systems in the stack are well overlapped, so this complex can be considered as *H*-aggregate. This structure is similar to structures **2.1**–**2.3**, but the third polyphosphate strand is added that binds to the heads of porphyrins. Some of the calculated structures are presented in Fig. 9.

We were unable to localize energetically favorable parallel $TMPyP^{3+}$ arrays with a slipped stacking, i.e. strong horizontal shift (parallel *J*-aggregates). At the same time, antiparallel structures were found with either horizontal or radial shift of porphyrin planes. While in parallel complexes three PPS chains are easily arranged around the porphyrin aggregates, in "face-to-face" antiparallel structures, the porphyrin stacks can in principle interact with four polyphosphate chains, two of them are bound at the sides of the aggregates and two at their head/tail regions.

In all cases, phosphate negative charges of PPS bound to $TMPyP^{3+}$ stacks are neutralized by porphyrin cationic groups. It should be noted that PPS chains in modeled complexes do not adopt a single conformations, e.g. all-*trans* where the electrostatic repulsion of anionic groups is minimized (Fig. 7A); on the contrary, a combination of *cis*- and *trans*-orientations of phosphate groups in PPS is usually observed, and this flexibility allows the formation of energetically most favorable complexes. Nevertheless, in all cases only every second phosphate group interacts with the sides of porphyrin stack, whereas half of phosphate anions which are not oriented to porphyrins remain unbound and thus free for the interactions with other cationic molecules (Fig. 7B). Even lower fraction of phosphate anions (every fourth) binds to the head/tail regions of antiparallel structures where charged heads and uncharged tails alternate. Free phosphates may bind to other porphyrin molecules, so it is possible to arrange two porphyrin stacks on a single PPS (Fig. 7C). Moreover, the formation of extended 3-dimensional aggregates of very complex nature is possible. We did not try to calculate such structures as they are too complicated for the DFT method.

We have calculated using a DFT method the total energies of porphyrin-PPS assemblies in water. Taking the total energy of complex **1.1** for zero, the values of relative energies for complexes **1.2**, **1.3**, **2.1**, **2.2** and **2.3** are equal to 56.94, 14.86, 7.15, 63.88 and 78.55 kcal/mol, respectively (see Supplementary material, Table S1). The obtained data

suggest that the most favorable structure among the complexes with two PPS chains is complex **1.1** with antiparallel orientation and a slight radial turn of porphyrin rings relative to each other, i.e. *H*-aggregate (Fig. 9). Somewhat less favorable structures are parallel complex **2.1** with no horizontal shift but with a radial turn of porphyrin rings similar to that in **1.1**, and antiparallel complex **1.3** with a significant horizontal shift of porphyrins (*J*-aggregate). The other possible assemblies containing two PPS chains (**1.2**, **2.2**, **2.3**) are less probable. The parallel structure **3.1** containing three polyphosphate strands also seems to be favorable, however, direct comparison of the calculation data obtained for very different structures containing 2 and 3 polyphosphate chains and different total charges is rather incorrect.

Thus, DFT calculations allowed finding several possible types of polyphosphate-templated π-stacking *H*- and *J*-aggregates of tricationic porphyrin $TMPyP^{3+}$ stacks formed in aqueous solutions. The results of molecular modeling are in good agreement with our experimental data suggesting the presence of both types of aggregates in the studied mixtures.

3.5. Comparison between PPS-induced aggregation of $TMPyP^{3+}$ and TMPyP4

The experimentally obtained spectroscopic data were compared with those previously published for TMPyP4–PPS system [17] to determine similarities and differences in the behavior of these two porphyrins under their binding to inorganic polyphosphate. The functionalization of TMPyP4 porphyrin to $TMPyP^{3+}$ via the attachment of carboxyalkyl side chain reduces the number of its positively charged groups from 4 to 3 (see Fig. 1A), lowers the chromophore symmetry and affects the spatial structure of the aggregates formed on oppositely charged polymeric matrix. The modification practically does not influence the shape of the free porphyrin spectra (only ~3 nm red shifts of Soret absorption and fluorescence bands are observed for $TMPyP^{3+}$ in comparison with TMPyP4 ones). However, the addition of inorganic polyphosphate induces strongly different changes in the absorption of these dyes. So, for TMPyP4 compound the 51% hypochromism and 12 nm blue shift of Soret band were registered at low *P*/*D* values corresponding to stoichiometric binding conditions, whereas in the case of $TMPyP^{3+}$ the band maximum is 11 nm red-shifted, 53% hypochromism is observed and the band becomes structured. Spectral deconvolution performed has shown that the last one is the sum of two bands with maxima at 443 and 415 nm. In contrast, almost the same changes in the fluorescence behavior were registered for both compounds in the initial *P*/*D* region during the titration experiment. Strong quenching of the porphyrin emission linearly dependent on PPS concentration, as well as increase in their fluorescence polarization degree were registered evidencing cooperative binding mechanism. The shift of the titration curve minimum from $P/D = 5.3$ for TMPyP4 to $P/D = 3.5$ for $TMPyP^{3+}$ is conditioned by the change in the number of positively charged groups from 4 to 3. Under the stoichiometric binding conditions the minimal levels of the porphyrin emission were registered being amounted to 23% from initial for TMPyP4 and 12.5% for $TMPyP^{3+}$ evidencing formation of highly-ordered structures. For both compounds the above mentioned transformations are accompanied by the splitting of the fluorescence band and the appearance of strong light scattering. The maximal scattering was registered under *P*/*D* values corresponding to the saturation of the binding near the titration curve minima. For tricationic porphyrin–polyphosphate complex the maximal scattering signal is more than twice as high as that for tetracationic one (70,000 cps and 43,000 cps correspondingly). However the increase of *P*/*D* value is accompanied by the different behavior of their fluorescence and scattering. For TMPyP4 the scattering signal decreases gradually, so that at $P/D = 1000$ its intensity is approximately 2300 cps, and at $P/D > 2000$ it becomes only twice as much as the signal for the solution without PPS that evidences the aggregate disintegration. In contrast, aggregates formed in the $TMPyP^{3+}$–PPS system are very stable. At $P/D = 1000$ the LS signal amounts to 30,000 cps (not shown). For tricationic porphyrin–polyphosphate complex the fluorescence band recorded at $P/D = 1200$ remains splitted, whereas for tetracationic one it has an unstructured shape, as for the free dye. As compared to the emission of free porphyrin, the fluorescence intensities are 40% for $TMPyP^{3+}$–PPS complex and 80% for TMPy4–PPS one (calculated as ratio between the areas of corresponding emission bands), their fluorescence polarization degrees are 0.065 and 0.034, respectively. It is obvious that the size and shape of the aggregates formed under the stoichiometric binding of these porphyrins to PPS are also different. From analysis of the absorption spectra transformation we have concluded that in the case of $TMPyP^{3+}$–PPS system the aggregates constitute the mixture of *J*- and *H*-types. Their size estimated from light scattering data is about several hundred nanometers, whereas for TMPyP4–PPS only columnar H-aggregates are formed being approximately 14 nm in length.

4. Conclusions

Formation of the $TMPyP^{3+}$ self-assemblies in water is revealed under the porphyrin binding to inorganic polyphosphate. The changes in the Soret absorbance band evidence that both *J*- and *H*-type aggregates form simultaneously. The aggregation results in the eight-fold quenching of porphyrin fluorescence. According to molecular modeling data, the porphyrin molecules can be arranged in spiral-like (either parallel or antiparallel) or "face-to-face" antiparallel structures, with possible formation of two porphyrin stacks at the polyanionic matrix of each PPS strand. The ability of each PPS strand to be a template for formation of two columnar porphyrin stacks results in the integration of the adjacent stacks into higher-order aggregates. Their size estimated from the light scattering data reaches *ca.* 320 nm in the case of spherical particles, and *ca.* 580 nm for polydisperse coils. As compared to TMPyP4 aggregates formed on PPS under the similar experimental conditions [17], those for tricationic porphyrin are substantially more stable and extended.

Acknowledgments

Authors are grateful to Professor J. Leszczynski (Department of Chemistry, Jackson State University, USA) for providing access to computational resources. This research was partially supported by the State program of Ukraine "Nanotechnologies and nanomaterials" (project No. 5.16.3.36).

Appendix A. Supplementary data

Supplementary data to this article can be found online at http://dx.doi.org/10.1016/j.bpc.2013.11.006.

References

[1] C.M. Drain, J.T. Hupp, K.S. Suslick, M.R. Wasilewski, X. Chen, A perspective on four new porphyrin-based functional materials and devices, J. Porphyrins Phthalocyanines 6 (2002) 243–258, http://dx.doi.org/10.1142/S1088424602000282.
[2] J.A.A.W. Elemans, R. van Hameren, R.J.M. Nolte, A.E. Rowan, Molecular materials by self-assembly of porphyrins, phthalocyanines, and perylenes, Adv. Mater. 18 (2006) 1251–1266, http://dx.doi.org/10.1002/adma.200502498.
[3] I.M. Dixon, F. Lopez, J.-P. Esteve, A.M. Tejera, M.A. Blasco, G. Pratviel, B. Meunier, Porphyrin derivatives for telomere binding and telomerase inhibition, ChemBioChem 6 (2005) 123–132, http://dx.doi.org/10.1002/cbic.200400113.
[4] Y. Takeshi, U. Tadayuki, I. Yoshinobu, Stabilization of guanine quadruplex DNA by the binding of porphyrins with cationic side arms, Bioorg. Med. Chem. 13 (2005) 2423–2430, http://dx.doi.org/10.1016/j.bmc.2005.01.041.
[5] P. Zhao, L.-C. Hu, J.-W. Huang, D. Fu, H.-C. Yu, L.-N. Ji, Cationic porphyrin–anthraquinone dyads: modes of interaction with G-quadruplex DNA, Dyes Pigments 83 (2009) 81–87, http://dx.doi.org/10.1016/j.dyepig.2009.03.015.
[6] B. Mestre, G. Pratviel, B. Meunier, Preparation and nuclease activity of hybrid "metallotris(methylpyridinium)porphyrin oligonucleotide" molecules having a 3′-loop for protection against 3′-exonucleases, Bioconjug. Chem. 6 (1995) 466–472, http://dx.doi.org/10.1021/bc00034a017.

[7] I. Dubey, G. Pratviel, B. Meunier, Synthesis and DNA cleavage of 2′-O-amino-linked metalloporphyrin–oligonucleotide conjugates, J. Chem. Soc. Perkin Trans. 1 (2000) 3088–3095, http://dx.doi.org/10.1039/B004431H.
[8] P. Zhao, L.-C. Hu, J.-W. Huang, K.-C. Zheng, J. Liu, H.-C. Yu, L.-N. Ji, DNA binding and photocleavage properties of a novel cationic porphyrin–anthraquinone hybrid, Biophys. Chem. 134 (2008) 72–83, http://dx.doi.org/10.1016/j.bpc.2008.01.009.
[9] P. Zhao, J.-W. Huang, W.-J. Mei, J. He, L.-N. Ji, DNA binding and photocleavage specificities of a group of tricationic metalloporphyrins, Spectrochim. Acta A 75 (2010) 1108–1114, http://dx.doi.org/10.1016/j.saa.2009.12.065.
[10] E. Izbicka, R.T. Wheelhouse, E. Raymond, K.K. Davidson, R.A. Lawrence, D. Sun, B.E. Windle, L.H. Hurley, D.D. Von Hoff, Effects of cationic porphyrins as G-quadruplex interactive agents in human tumor cells, Cancer Res. 59 (1999) 639–644(PubMed: 9973212).
[11] Y. Xu, Chemistry in human telomere biology: structure, function and targeting of telomere DNA/RNA, Chem. Soc. Rev. 40 (2011) 2719–2740, http://dx.doi.org/10.1039/C0CS00134A.
[12] V.V. Negrutska, L.V. Dubey, M.M. Ilchenko, I.Ya. Dubey, Design and study of telomerase inhibitors based on G-quadruplex ligands, Biopolym. Cell 29 (2013) 169–176, http://dx.doi.org/10.7124/bc.000817.
[13] J.S. Lee, J. Feijen, Polymersomes for drug delivery: design, formation and characterization, J. Control. Release 161 (2) (2012) 473–483, http://dx.doi.org/10.1016/j.jconrel.2011.10.005.
[14] R.F. Pasternack, C. Bustamante, P.J. Collngs, A. Giannetto, E.J. Gibbs, Porphyrin assemblies on DNA as studied by a resonance light-scattering technique, J. Am. Chem. Soc. 115 (1993) 5393–5399, http://dx.doi.org/10.1021/ja00066a006.
[15] R.F. Pasternack, J.I. Goldsmith, S. Szep, E.J. Gibbs, A spectroscopic and thermodynamic study of porphyrin/DNA supramolecular assemblies, Biophys. J. 75 (1998) 1024–1031, http://dx.doi.org/10.1016/S0006-3495(98)77591-5.
[16] I. Sazanovich, A. Panarin, A. Stupak, S. Terekhov, V. Chirvony, Fluorescence properties of the dicationic porphyrin 5,15-DiMPyP orderly aggregated along DNA surface, Photochem. Photobiol. Sci. 7 (2008) 1091–1098, http://dx.doi.org/10.1039/B806282J.
[17] V.N. Zozulya, O.A. Ryazanova, I.M. Voloshin, A.Yu. Glamazda, V.A. Karachevtsev, Spectroscopic detection of tetracationic porphyrin H-aggregation on polyanionic matrix of inorganic polyphosphate, J. Fluoresc. 20 (2010) 695–702, http://dx.doi.org/10.1007/s10895-010-0609-1.
[18] C. Casas, B. Saint-Jalmes, C. Loup, C.J. Lacey, B. Meunier, Synthesis of cationic metalloporphyrin precursors related to the design of DNA cleavers, J. Org. Chem. 58 (1993) 2913–2917, http://dx.doi.org/10.1021/jo00062a045.
[19] Y. Zhao, D.G. Truhlar, Comparative DFT study of van der Waals complexes: rare-gas dimers, alkaline-earth dimers, zinc dimer, and zinc-rare-gas dimers, J. Phys. Chem. A 110 (2006) 5121–5129, http://dx.doi.org/10.1021/jp060231d.
[20] http://www.mcsr.olemiss.edu.
[21] V. Barone, M. Cossi, Quantum calculation of molecular energies and energy gradients in solution by a conductor solvent model, J. Phys. Chem. A 102 (1998) 1995–2001, http://dx.doi.org/10.1021/jp9716997.
[22] M. Cossi, G. Scalmani, N. Rega, V. Barone, New developments in the polarizable continuum model for quantum mechanical and classical calculations on molecules in solution, J. Chem. Phys. 117 (2002) 43–54, http://dx.doi.org/10.1063/1.1480445.
[23] G. Schwarz, S. Klose, Thermodynamic and kinetic studies on the cooperative binding of proflavine to linear polyanions, Eur. J. Biochem. 29 (1972) 249–256, http://dx.doi.org/10.1111/j.1432-1033.1972.tb01981.x.
[24] V.N. Zozulya, I.M. Voloshin, Cooperative binding of quinacrine to inorganic polyphosphate, Biophys. Chem. 48 (1994) 353–358, http://dx.doi.org/10.1016/0301-4622(93)E0047-9.
[25] G. Schwarz, Cooperative binding to linear biopolymers. 1. Fundamental static and dynamic properties, Eur. J. Biochem. 12 (1970) 442–453, http://dx.doi.org/10.1111/j.1432-1033.1970.tb00871.x.
[26] P.V. Bohn, Aspects of structure and energy transport in artificial molecular assemblies, Annu. Rev. Phys. Chem. 44 (1993) 37–60, http://dx.doi.org/10.1146/annurev.pc.44.100193.000345.
[27] F.J. Vergeldt, R.B.M. Koehorst, A. van Hoek, T.J. Schaafsma, Intramolecular interactions in the ground and excited state of tetrakis(N-methylpyridyl)porphyrins, J. Phys. Chem. 99 (1995) 4397–4405, http://dx.doi.org/10.1021/j100013a007.
[28] N.C. Maiti, S. Mazumdar, N. Periasamy, J- and H-aggregates of porphyrins with surfactants: fluorescence, stopped flow and electron microscopy studies, J. Porphyrins Phthalocyanines 2 (1998) 369–376, http://dx.doi.org/10.1002/(SICI)1099-1409(199807/10)2:4/5<369::AID-JPP92>3.0.CO;2-3.
[29] K. Šišková, B. Vlčková, P. Mojzeš, Spectral detection of J-aggregates of cationic porphyrin and investigation of conditions of their formation, J. Mol. Struct. 744–747 (2005) 265–272, http://dx.doi.org/10.1016/j.molstruc.2004.10.047.
[30] N. Blom, J. Odo, K. Nakamoto, D.P. Strommen, Resonance Raman studies of metal tetrakis(4-N-methylpyridyl)porphine: band assignments, structure-sensitive bands, and species equilibria, J. Phys. Chem. 90 (1986) 2847–2852, http://dx.doi.org/10.1021/j100404a015.
[31] J.H. Schneider, J. Odo, K. Nakamoto, Interactions of water-soluble metalloporphyrins with nucleic acids studied by resonance Raman spectroscopy, Nucleic Acids Res. 16 (1988) 10323–10338, http://dx.doi.org/10.1093/nar/16.21.10323.
[32] D.L. Akins, H.-R. Zhu, C. Guo, Aggregation of tetraaryl-substituted porphyrins in homogeneous solution, J. Phys. Chem. 100 (1996) 5420–5425, http://dx.doi.org/10.1021/jp951467c.
[33] C.A. Hunter, J.K.M. Sanders, The nature of π–π interactions, J. Am. Chem. Soc. 112 (1990) 5525–5534, http://dx.doi.org/10.1021/ja00170a016.
[34] P. Doty, R.F. Steiner, Light scattering and spectrophotometry of colloidal solutions, J. Chem. Phys. 18 (1950) 1211–1220, http://dx.doi.org/10.1063/1.1747913.
[35] Y. Zhao, D.G. Truhlar, The M06 suite of density functionals for main group thermochemistry, kinetics, noncovalent interactions, excited states, and transition elements: two new functionals and systematic testing of four M06 functionals and twelve other functionals, Theor. Chem. Acc. 120 (2008) 215–241, http://dx.doi.org/10.1007/s00214-007-0310-x.